



# Nitrogen-doped SrTiO<sub>3</sub>/TiO<sub>2</sub> composite photocatalysts for hydrogen production under visible light irradiation

Yan Jian-Hui<sup>a,b</sup>, Zhu Yi-Rong<sup>a,b,\*</sup>, Tang You-Gen<sup>a</sup>, Zheng Shu-Qin<sup>a,b</sup>

<sup>a</sup> Department of Chemistry and Chemical Engineering, Hunan Institute of Science and Technology, Yueyang 414000, China

<sup>b</sup> School of Chemistry and Chemical Engineering, Central South University, Changsha 410083, China

## ARTICLE INFO

### Article history:

Received 21 October 2007

Received in revised form 19 April 2008

Accepted 24 April 2008

Available online 10 June 2008

### Keywords:

Composite catalyst

Sol–gel

Photocatalytic

Nitrogen-doped

Hydrogen production

## ABSTRACT

Nitrogen-doped SrTiO<sub>3</sub> powders were prepared by solid phase method, and further combined with TiO<sub>2</sub> by sol–gel method. Then Pt particles were deposited to prepare Pt-loaded composite powders by hydrogen reduction method. These obtained powders were characterized by X-ray diffraction (XRD), scanning electron microscopy (SEM), Fourier transform infrared spectra, thermogravimetric–differential thermal, ultraviolet (UV)–vis diffuse reflectance spectra and fluorescence spectra techniques. Photocatalytic production of hydrogen from oxalic acid solution was used as the probe reaction to evaluate the photocatalytic activity of hydrogen production under visible light in detail from aspects of different calcination temperatures, and different contents of metal Pt. The result demonstrates that when the calcination temperature is 400 °C, the optimized photocatalytic activity of hydrogen production under visible light can be achieved. Pt depositing greatly improves the photocatalytic activity, and the average hydrogen production rate is up to 5.1 mmol g cat<sup>-1</sup> h<sup>-1</sup> with 2 wt.% loaded Pt.

© 2008 Elsevier B.V. All rights reserved.

## 1. Introduction

Energy and environment have become two important problems with the rapid development of industry. Photocatalytic reactions of semiconductor such as decomposition of water have been received great attention around the world [1,2]. SrTiO<sub>3</sub>, one of the important photocatalysts, has been used for water splitting and mineralization of organic pollutants under ultraviolet (UV) irradiation, whereas it is active only in the UV region because of its wide band gap (3.2 eV). Therefore, its photocatalytic properties in UV light range have been investigated for several decades [3,4]. Nowadays, the research on photocatalysis in the field of visible light has attracted many people's attention [5–9], and it has become a target of researchers to improve the photocatalytic activity of SrTiO<sub>3</sub> and extend its optical absorption edge towards the visible light range. To our knowledge, researches of SrTiO<sub>3</sub> on the photocatalytic hydrogen production are still scarce. We have not found any report on nitrogen-doped SrTiO<sub>3</sub>/TiO<sub>2</sub> photocatalyst under visible light irradiation.

In this paper, nitrogen-doped SrTiO<sub>3</sub> powders were prepared by solid phase method, and nitrogen-doped SrTiO<sub>3</sub>/TiO<sub>2</sub> composite powders were prepared by sol–gel method and then Pt powders

were further deposited to prepare Pt-loaded composite powders by hydrogen reduction method, whose photocatalytic activity for hydrogen production from oxalic acid solution was investigated under visible light irradiation. The effects of several factors such as the calcination temperatures of composite powders, and the contents of metal Pt on the rate of hydrogen production were studied.

## 2. Experimental

### 2.1. Preparation of photocatalysts

According to our previous research [10], the nitrogen-doped SrTiO<sub>3</sub> powders were prepared as follows: hexamethylenetetramine (HMT) was mixed with a perovskite SrTiO<sub>3</sub> powder and grinded thoroughly in an agate mortar. The mass ratio of hexamethylenetetramine to SrTiO<sub>3</sub> powders was 3 to 1. The mixed powder was packed in a lidded double alumina crucible and calcined at 450 °C under aerated conditions for 1 h. Nitrogen-doped SrTiO<sub>3</sub> powders obtained was grinded in mortar after calcination.

Nitrogen-doped SrTiO<sub>3</sub>/TiO<sub>2</sub> composite powders were prepared as follows: *tetra*-butyl titanate solution (10 ml) was added into anhydrous ethanol solution (20 ml) at room temperature under stirring, and the apparent slight yellowish solution was designated as A; the double distilled water (6 ml) and anhydrous ethanol solution (30 ml) were added into concentrated nitric acid (1.5 ml) under stirring, and the solution was designated as B. These two solutions were both continuously stirred for 15 min, then A solution was added dropwise (1 ml min<sup>-1</sup>) into B solution under vigorous stirring. After stirring for 2 h, nitrogen-doped SrTiO<sub>3</sub> powders were added (ensuring that the content of nitrogen-doped SrTiO<sub>3</sub> powders in composite catalysts is 30 wt.%) and stirred continuously for some time until the gel formed, which was allowed to stand at room temperature for a further 24 h to complete peptization. It was dried in vacuum conditions for 12 h, and then calcined at different temperatures for 1 h.

\* Corresponding author at: Department of Chemistry and Chemical Engineering, Hunan Institute of Science and Technology, Yueyang 414000, China.  
Tel.: +86 730 8648503; fax: +86 730 8640436.

E-mail address: [zhuyirong2004@163.com](mailto:zhuyirong2004@163.com) (Y.-R. Zhu).

Different contents of Pt-loaded nitrogen-doped SrTiO<sub>3</sub>/TiO<sub>2</sub> composite powders were prepared by impregnation hydrogen reduction method, and the required weight of nitrogen-doped SrTiO<sub>3</sub>/TiO<sub>2</sub> powders through ultrasonic treatment were added to different concentrations of chloroplatinic acid hexahydrate solution. This mixture solution obtained was stirred at an ambient temperature overnight, and dried in water at 373 K for several hours, and then the dried powders were transferred to tubular furnace. The samples were heated from room temperature to 673 K in a nitrogen atmosphere, and then maintained at 673 K for 2 h after the nitrogen atmosphere was replaced by hydrogen atmosphere, and finally cooled to room temperature under nitrogen atmosphere protection.

## 2.2. Characterization of photocatalysts

The X-ray diffraction (XRD) patterns of the samples were obtained on a Rigaku D/max 2550 VB<sup>+</sup> 18 kW X-ray diffractometer with Cu K $\alpha$  radiation at a scanning rate of 0.1° 2 $\theta$  s<sup>-1</sup>. The accelerating voltage and the applied current were 40 kV and 300 mA, respectively. The average crystallite sizes were determined according to the Scherrer equation. The surface morphologies of the samples were obtained from JEOL JSM-5600LV scanning electron microscopy (SEM). The chemical structure of the samples was examined using the Fourier transform infrared spectrophotometer (FT-IR, AVTATAR, 370) in the 400–4000 cm<sup>-1</sup> frequency range with KBr as a reference. Thermogravimetric and differential thermal (TG-DTA) patterns of the samples were recorded by using thermogravimetric-differential thermal analyzer to determine the temperature of possible decomposition and phase changes and the samples were heated at the rate of 10 °C min<sup>-1</sup> from room temperature to 1000 °C. The UV-vis spectroscopy of the samples was recorded on a UV-vis spectrophotometer (type 100-60) for the UV-vis absorption studies with wavelength range of 200–700 nm. Fluorescence spectrum (FS) was obtained with an LS-55 fluorescence spectrum spectrometer.

## 2.3. Photocatalytic experiments

The photocatalytic reaction was carried out in self-made tube-shaped quartz reactor including three layers connected with gas collecting devices, and water was used as the external circulation cooling and wind as the internal cooling. The reaction temperature was kept at 25 ± 0.2 °C by controlling the external circulation water in the water jacket of the reactor during the entire experiment. The photocatalyst powder (0.6 g) was dispersed by a magnetic stirrer in 600 ml aqueous solution containing 0.05 mol L<sup>-1</sup> oxalic acid as the sacrificial reagent. A 250-W xenon lamp was used as the light source. Before the irradiation, the reactor was deaerated with nitrogen for about 30 min, and the catalyst was kept in suspension state by a magnetic stirrer. The gas evolved was gathered by drainage method and analyzed by GC using a molecular sieve 13 $\times$  column and nitrogen as the carrier gas.

## 3. Results and discussion

### 3.1. Characterization of photocatalysts

XRD is used to investigate the phase structures of the samples. The XRD patterns of SrTiO<sub>3</sub>, N-SrTiO<sub>3</sub>, N-SrTiO<sub>3</sub>/TiO<sub>2</sub> (350–600 °C) and Pt/N-SrTiO<sub>3</sub>-TiO<sub>2</sub> (400 °C, 2 wt.%) are shown, respectively in Figs. 1(a) and (b) and 2(c)–(g) and (h). The average crystal size of SrTiO<sub>3</sub> was determined to be 38.8 nm and nitrogen-doped SrTiO<sub>3</sub> samples was 38.4 nm. The average crystal size of the TiO<sub>2</sub> single crystal in composite catalyst calcined at 350, 400, 450, 500 and 600 °C was determined to be 8.5, 9.1, 9.5, 11.8 and 12.6 nm, respectively. The size of the particles becomes bigger with the temperature rising, and this is confirmed by the XRD patterns in which the width of the diffraction peak is narrower and the shape of peak is sharper as the temperature rises. The results obtained were also agrees with those observed by SEM. The composite catalysts mainly consist of anatase TiO<sub>2</sub> and SrTiO<sub>3</sub>. From Fig. 2(g) we can observe that no peak of rutile phase TiO<sub>2</sub> is observed after being calcined at 600 °C (g), which illustrates that the combination of nitrogen-doped SrTiO<sub>3</sub> with TiO<sub>2</sub> inhibits the crystal transformation of TiO<sub>2</sub> in composite catalyst to some extent. In addition, the peaks of nitrogen and platinum are not observed either from Figs. 1 and 2, and this may be due to the low dopant content of nitrogen and platinum beyond the minimum detection limit of XRD.

The SEM micrographs of the nitrogen-doped SrTiO<sub>3</sub> and Pt-loaded nitrogen-doped SrTiO<sub>3</sub>/TiO<sub>2</sub> (400 °C, 2 wt.%) are shown in Fig. 3(a) and (b). From Fig. 3(a), the particles of nitrogen-doped

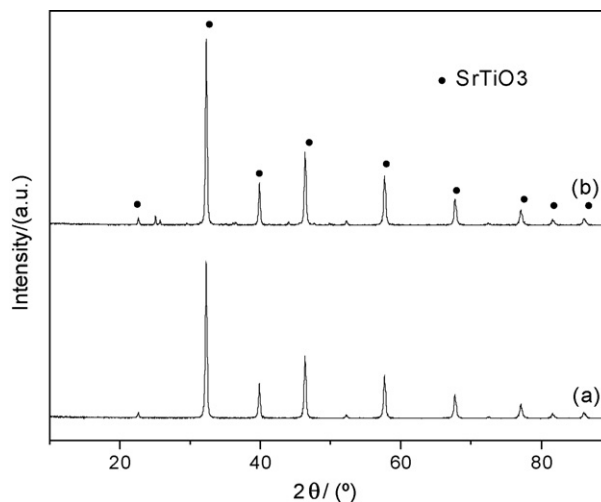


Fig. 1. XRD patterns of the samples: (a) SrTiO<sub>3</sub> and (b) N-SrTiO<sub>3</sub>.

SrTiO<sub>3</sub> are of small spherical shape. They have homogeneous distributions and only a fraction of agglomeration, and the surface morphologies are similar to those of pure SrTiO<sub>3</sub> powders. As shown in Fig. 3(b), the as-prepared composite catalyst is irregularly spherical and its particle sizes are not identical. Some large particles are nitrogen-doped SrTiO<sub>3</sub> whose surfaces were covered by tiny TiO<sub>2</sub> particles to form a heterogeneous core-shell structure, furthermore, the surface of particles is not smooth, which offers a good site for the photocatalytic reaction. The surface morphology of Pt-loaded composite catalyst is similar to that of unloaded one, and no Pt particles are observed mainly because of low Pt content.

Fig. 4 displays the Fourier transform infrared spectra of TiO<sub>2</sub> (400 °C), nitrogen-doped SrTiO<sub>3</sub> and nitrogen-doped SrTiO<sub>3</sub>/TiO<sub>2</sub> (600 °C). From the FT-IR spectrum of TiO<sub>2</sub>, the peaks of 3420 and 1630 cm<sup>-1</sup> correspond to the stretching vibrations of O–H and bending vibrations of adsorbed water molecules, respectively, indicating the existence of O–H on the surface of TiO<sub>2</sub>. The stretching vibrations of Ti–O are not observed due to the coverage of strong absorption band in the range of 750–450 cm<sup>-1</sup>. From the FT-IR spectrum of nitrogen-doped SrTiO<sub>3</sub>, the peak of 3440 cm<sup>-1</sup> corresponds to the stretching vibrations of adsorbed water O–H, and the absorption peak of 1458 cm<sup>-1</sup> is probably caused by the residual organic compounds coming from the process of nitrogen doping. The strong

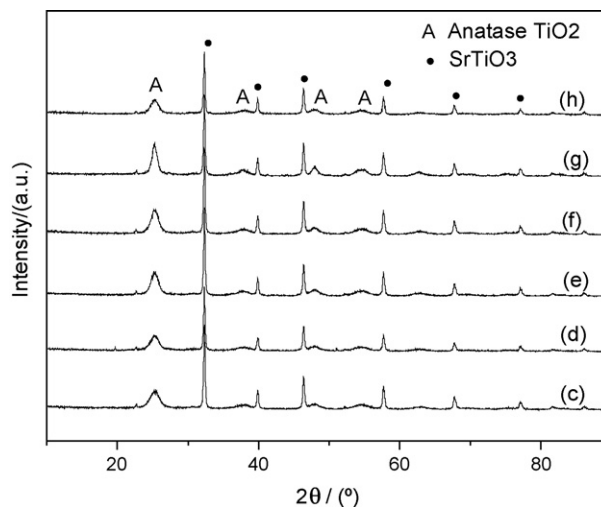


Fig. 2. XRD patterns of the samples: (c–g) N-SrTiO<sub>3</sub>/TiO<sub>2</sub> and (h) Pt/N-SrTiO<sub>3</sub>-TiO<sub>2</sub>.

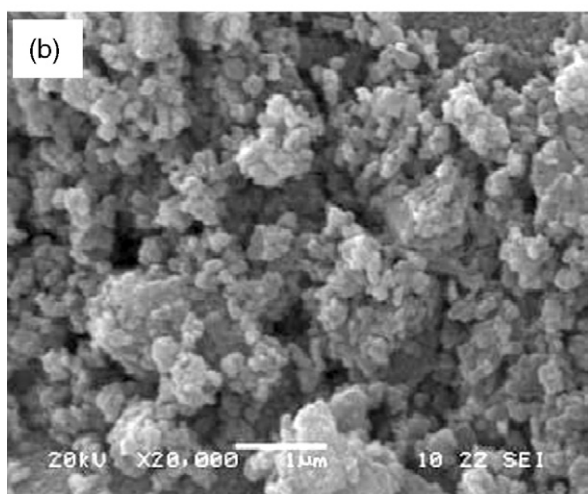
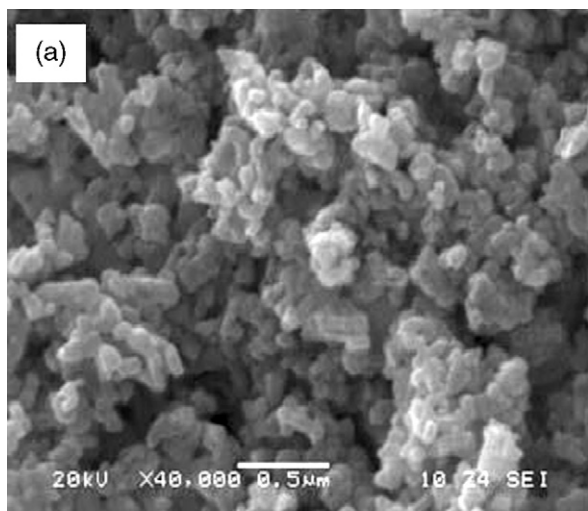


Fig. 3. SEM patterns of the samples: (a) N-SrTiO<sub>3</sub> and (b) Pt/N-SrTiO<sub>3</sub>/TiO<sub>2</sub>.

broad absorption peak in the range of 3100–3450 cm<sup>-1</sup> corresponds to the O–H stretching vibrations of the nitrogen-doped SrTiO<sub>3</sub>/TiO<sub>2</sub> composite samples, which indicates that the two different semiconductors interact with each other after combination, resulting in existence of more O–H on the surface of composite catalysts.

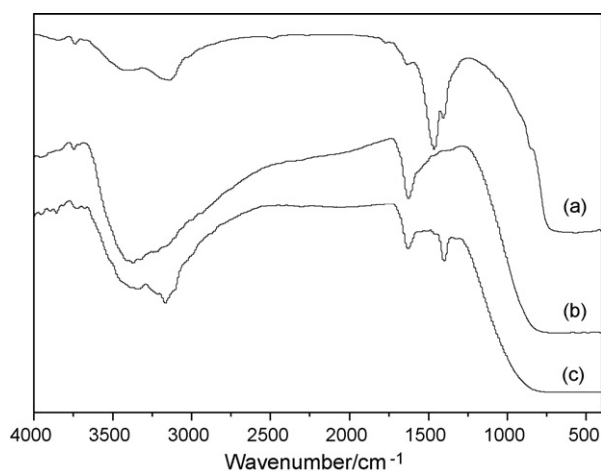


Fig. 4. Infrared spectra of the samples: (a) N-SrTiO<sub>3</sub>, (b) TiO<sub>2</sub> and (c) N-SrTiO<sub>3</sub>/TiO<sub>2</sub>.

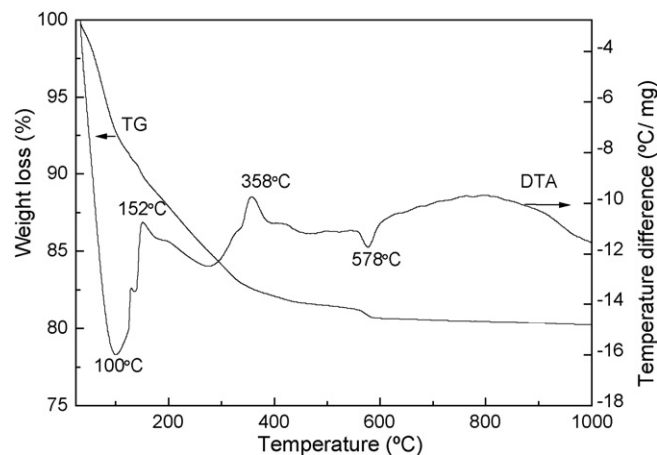


Fig. 5. TG-DTA curve of N-SrTiO<sub>3</sub>/TiO<sub>2</sub> gel.

At the same time, the absorption peak near 1400 cm<sup>-1</sup> is due to the Ti–O–Ti vibration [11], which further shows the interaction of the two different semiconductors after combination. However, this peak is not observed on the single sample of nitrogen-doped SrTiO<sub>3</sub> and TiO<sub>2</sub> from the FT-IR spectra.

Fig. 5 shows the TG-DTA curve of nitrogen-doped SrTiO<sub>3</sub>/TiO<sub>2</sub> dry gel. From the differential thermal curve, the strong endothermic peak at about 100 °C is due to the free adsorbed water of the gel and the volatilization of organic solvents such as ethanol and acetic acid [12], meanwhile the corresponding weight loss is observed from the thermogravimetric curve. The first exothermic peak at 152 °C is due to the decomposition of the residual organic compounds; the second exothermic peak at 358 °C corresponds to the crystallization of the amorphous phase TiO<sub>2</sub> into the anatase phase. In addition, the appearance of another endothermic peak and slight weight loss of the thermogravimetric curve at about 578 °C are perhaps owing to the transformation of the anatase phase TiO<sub>2</sub> into the anatase phase, besides, the possibility of the so-called heterojunction energy effects caused by the combination of two different oxides could not be ruled out.

Fig. 6 displays the UV-vis absorption spectra of SrTiO<sub>3</sub>, N-SrTiO<sub>3</sub>, N-SrTiO<sub>3</sub>/TiO<sub>2</sub> (400 °C) and Pt/N-SrTiO<sub>3</sub>/TiO<sub>2</sub> (400 °C, 2 wt.%). From Fig. 6, the absorption intensity of the samples is almost the same in UV light range, whereas it is evidently differ-

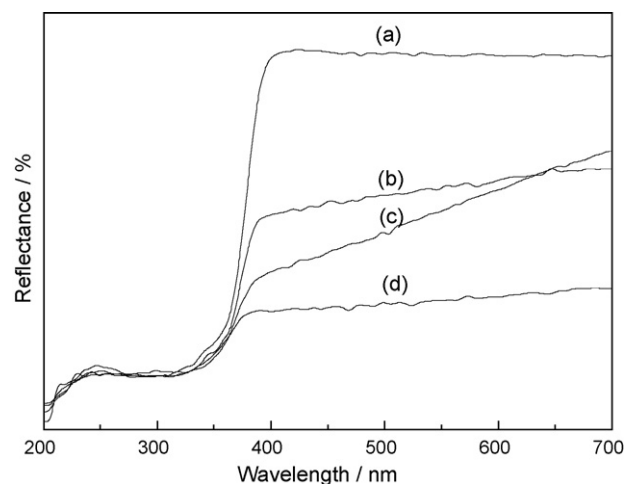


Fig. 6. UV-vis diffuse reflectance spectra of the samples: (a) SrTiO<sub>3</sub>, (b) N-SrTiO<sub>3</sub>, (c) N-SrTiO<sub>3</sub>/TiO<sub>2</sub> and (d) Pt/N-SrTiO<sub>3</sub>/TiO<sub>2</sub>.

ent in visible light range. The diffuse reflectance rate of SrTiO<sub>3</sub> is appropriate to 100% in the range of 400–700 nm, namely, it shows no absorption for the visible light. While the diffuse reflectance rate of modified SrTiO<sub>3</sub> evidently decreased, and it shows rather strong absorption for the visible light. After SrTiO<sub>3</sub> was doped by nitrogen, the replacing O<sup>2-</sup> with N<sup>3-</sup> would result in the formation of anion defects for the charge compensation, and the anion defects seemed to lead to high visible light absorption ability of the sample, according to Justicia et al.'s work [13]. When the nitrogen-doped SrTiO<sub>3</sub> combines with TiO<sub>2</sub>, the interaction occurs between the two different semiconductor oxides, and the visible light absorption ability is further enhanced compared to nitrogen-doped SrTiO<sub>3</sub> so that it is favorable for the improvement of the photocatalytic activity. UV–vis diffuse reflectance spectrum is also a common method used to track the formation of metal nanoparticles. The visible light absorption of the composite catalysts loaded by Pt is significantly enhanced. According to literature [14], it results from the contribution of metal nanoparticles plasma absorption peak, whereas the different plasma absorption peaks are caused by many reasons, mainly including the size and shape of deposited metal particles, surface electron density of the metal particles and property of medium for metal deposition. It is also demonstrated in experiment that nitrogen doping, combination of different semiconductors and deposition of noble metal all contribute to the enhancement of absorption for the visible light.

Fluorescence spectrum is an effective method for researching on the electronic structure and optical properties of the semiconductor nanoparticles as well as showing the information of oxygen vacancy or defects of material surface and the separation and recombination of photo-generated carriers [15,16]. The fluorescence spectrum intensity determines the number of electron–hole recombination. A large number of electrons and holes generate after the excitement of photocatalysts under visible light irradiation and only a fraction of them recombine rapidly. Their energy is released in the form of fluorescence, and high fluorescence spectrum intensity means high electron–hole pair recombination rate and poor photocatalytic activity. Fig. 7 displays the fluorescence spectra of SrTiO<sub>3</sub>, N–SrTiO<sub>3</sub>, TiO<sub>2</sub> (400 °C), N–SrTiO<sub>3</sub>/TiO<sub>2</sub> (400 °C), and Pt/N–SrTiO<sub>3</sub>/TiO<sub>2</sub> (400 °C, 2 wt.%). As shown in Fig. 7, the fluorescence spectrum intensities of SrTiO<sub>3</sub> and TiO<sub>2</sub> are relatively higher, which illustrates that the photo-induced electrons and holes are easy to recombine together. The fluorescence spectrum intensity of nitrogen-doped SrTiO<sub>3</sub> decreases slightly, showing that the appropriate content of doped nitrogen facilitates the effective sep-

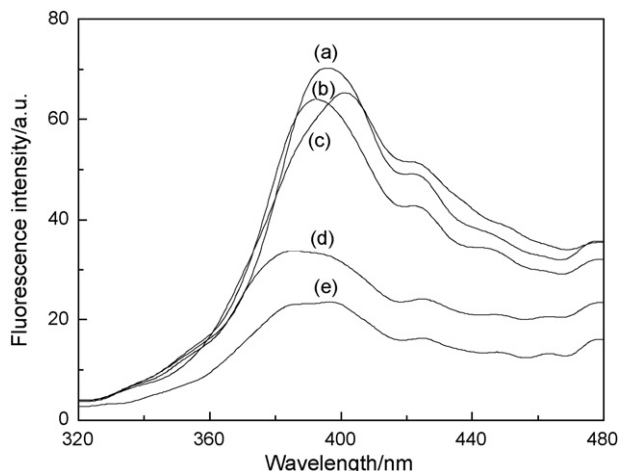


Fig. 7. Fluorescence spectra of the samples: (a) SrTiO<sub>3</sub>, (b) N–SrTiO<sub>3</sub>, (c) TiO<sub>2</sub>, (d) N–SrTiO<sub>3</sub>/TiO<sub>2</sub> and (e) Pt/N–SrTiO<sub>3</sub>/TiO<sub>2</sub>.

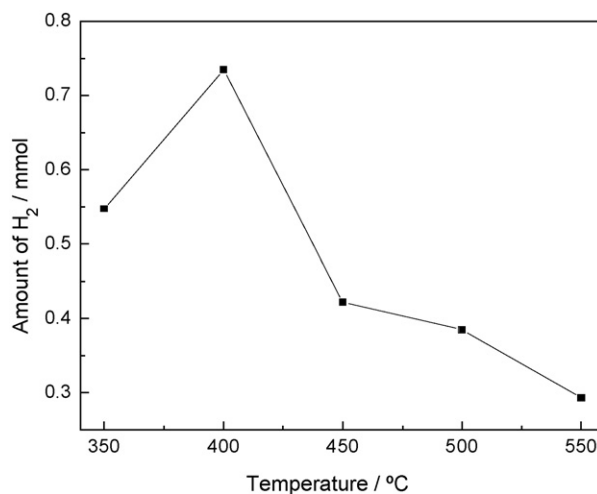


Fig. 8. Photocatalytic hydrogen production activity of N–SrTiO<sub>3</sub>/TiO<sub>2</sub> calcined at different temperatures.

aration of photo-generated electron–hole pair since the replacing O<sup>2-</sup> with N<sup>3-</sup> will result in the formation of oxygen vacancies, and the appropriate oxygen vacancies can inhibit the recombination of photo-generated charge to some extent [17]. The fluorescence spectrum intensity of nitrogen-doped SrTiO<sub>3</sub>/TiO<sub>2</sub> decrease greatly, illustrating that the combination of nitrogen-doped SrTiO<sub>3</sub> with TiO<sub>2</sub> forms the heterojunction structure, which becomes the convenient channel for the transfer of photo-generated electrons and holes in the process of photocatalytic reaction because of its special energy band structure and transport characteristics of carriers, leading to the effective separation of photo-generated carriers, the reduction of electron–hole recombination, and thus the photocatalytic activity improves [18,19]. The fluorescence spectrum intensity further decreases after depositing Pt, which indicates that the deposition of Pt plays a competitive role in capturing the photoelectron, and results in the separation of photo-generated electron–hole pairs, the reduction of photo-generated carriers recombination, therefore, the photocatalytic activity enhances. The order of fluorescence spectrum intensity agrees with that of photocatalytic activity obtained by our experiments.

### 3.2. Photocatalytic activity of photocatalysts

Photocatalytic hydrogen production activity of nitrogen-doped SrTiO<sub>3</sub>/TiO<sub>2</sub> composite samples calcined at different temperatures under visible light irradiation is shown in Fig. 8. From Fig. 8, we can see that the photocatalytic hydrogen production activity assumes the law of increasing first and decreasing last with calcination temperature rising, and the highest photocatalytic hydrogen production activity is achieved when the calcination temperature is 400 °C. The reason is that the amorphous TiO<sub>2</sub> with low activity is not completely transformed into the anatase TiO<sub>2</sub> with high activity when the calcination temperature is below 400 °C, which is confirmed by the TG–DTA and XRD analysis. In addition, a certain amount of organic substance carbon remained in the sample leads to the reduction of the photocatalytic activity. When the calcination temperature is above 400 °C, nitrogen element is oxidized into nitrogen oxides gas which releases into air with the rising of calcination temperature, and thus the nitrogen content doped in the sample decreases, weakening the effect caused by visible light irradiation. On the other hand, as the calcination temperature rises, the size of particles becomes larger, and the specific surface area becomes smaller, which are unfavorable for the generation

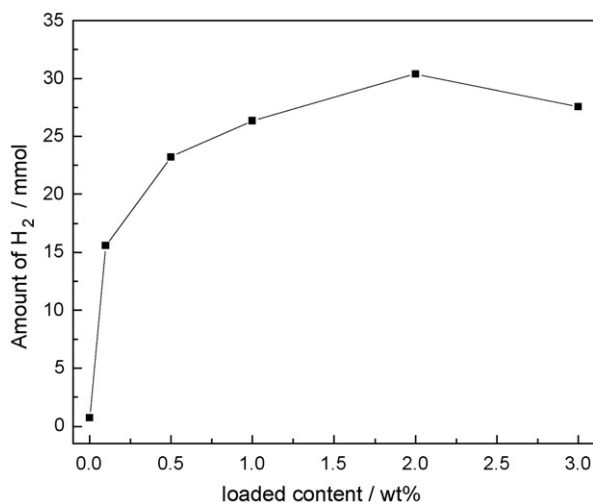


Fig. 9. Photocatalytic hydrogen production activity of different contents of Pt deposited N-SrTiO<sub>3</sub>/TiO<sub>2</sub>.

of photo-generated carriers, adsorption of sacrificial agent on the surface of catalyst and absorption of visible light, therefore, the photocatalytic activity decreases.

Fig. 9 illustrates the photocatalytic hydrogen production activity of nitrogen-doped SrTiO<sub>3</sub>/TiO<sub>2</sub> (400 °C) samples deposited with different contents of Pt under visible light irradiation. As shown in Fig. 9, the photocatalytic hydrogen production activity assumes the law of increasing first and decreasing last with loaded Pt increasing, and the highest photocatalytic hydrogen production activity is achieved when the amount of loaded Pt is 2 wt.%. The reason for this is as follows: when the composite semiconductor is loaded by a certain amount of Pt, and if the content of Pt is controlled within a suitable range, these metal Pt crystal nucleus and composite semiconductor systems can be regarded as an ultramicroclosed-circuit photoelectrochemical cell, and the electrons and holes generated by light irradiation are, respectively localized at metal Pt and composite semiconductor. The enrichment of electrons on metal Pt, and generation of holes on the surface of composite semiconductors leads to the separation of the electrons and holes and the declining probability of electron-hole pair recombination, consequently the photocatalytic activity of photocatalyst improves. When the content of loaded Pt is too low, the size of Pt particles covered on the surface of catalyst is small and Pt is uniformly dispersed, however, the small amount of loaded Pt may cause the failure of effective electron-hole pair separation and thus lead to the low photocatalytic activity; when the content of loaded Pt is too high, loaded

Pt particles covered on the surface of catalyst become more, and owing to the aggregation of Pt particles, larger size Pt clusters form, which can scatter the visible light, leading to the failure to trigger the composite catalyst covered by Pt effectively under visible light irradiation and the decreasing of electrons and holes, as a result, the photocatalytic activity decreases [20,21].

#### 4. Conclusions

No hydrogen was produced for single SrTiO<sub>3</sub> and TiO<sub>2</sub> under visible light irradiation. SrTiO<sub>3</sub> was doped nitrogen by solid phase method and further combined with TiO<sub>2</sub> by sol-gel method. The photocatalytic hydrogen production activity was greatly improved under visible light irradiation. When the temperature of calcination is 400 °C, the optimized photocatalytic activity of hydrogen production under visible light irradiation can be achieved. Pt depositing greatly improved the photocatalytic activity, and the average hydrogen production rate is up to 5.1 mmol g cat<sup>-1</sup> h<sup>-1</sup> with 2 wt.% loaded Pt.

#### Acknowledgement

This research was financially supported by National Nature Science Foundation of China (No. 20876039), and the Scientific Research Foundation of Hunan Provincial Education Department, China (No. 08A026).

#### References

- [1] A. Fujishima, K. Honda, *Nature* 238 (1972) 37.
- [2] A. Linsebigler, G. Lu, J.T. Yates, *Chem. Rev.* 95 (1995) 735.
- [3] G.B. Wang, Y.J. Wang, B.J. Song, Y.Q. Xu, *Chin. J. Inorg. Chem.* 19 (2003) 988.
- [4] M. Avudaithai, T.R.N. Kutty, *Mater. Res. Bull.* 22 (1987) 641.
- [5] H.T. Zhang, X.B. Wu, Y.M. Wang, *J. Phys. Chem. Solids* 68 (2007) 280.
- [6] T. Ohno, T. Tsubota, Y. Nakamura, K. Sayama, *Appl. Catal. A: Gen.* 288 (2005) 74.
- [7] J.S. Wang, S. Yin, M. Komatsu, Q.W. Zhang, F. Saito, T. Sato, *J. Photochem. Photobiol. A: Chem.* 165 (2004) 149.
- [8] T. Lshii, H. Kato, A. Kudo, *J. Photochem. Photobiol. A: Chem.* 163 (2004) 181.
- [9] M. Miyauchi, M. Takashio, H. Tobimatsu, *Langmuir* 20 (2004) 232.
- [10] Y.R. Zhu, Y.G. Tang, J.H. Yan, Q. Liu, *J. Inorg. Mater.* 23 (2008) (in press).
- [11] S.H. Zhong, J.H. Wang, *Petrochem. Technol.* 22 (1993) 307.
- [12] J.G. Yu, X.J. Zhao, *J. Inorg. Mater.* 15 (2000) 347.
- [13] I. Justicia, P. Ordejon, G. Canto, J.L. Mozos, J. Frasedas, G.A. Battiston, R. Gerbasi, A. Figueras, *Adv. Mater.* 19 (2002) 1399.
- [14] A. Henglein, *J. Phys. Chem.* 97 (1993) 5457.
- [15] X.Z. Li, F.B. Li, C.L. Yang, *J. Photochem. Photobiol. A: Chem.* 141 (2001) 209.
- [16] L. Foress, M. Schubnnell, *J. Appl. Phys. B* 56 (1993) 363.
- [17] H. Irie, Y. Watanabe, K. Hashimoto, *J. Phys. Chem. B* 107 (2003) 548.
- [18] M. Ueda, S. Otsuka-Yao-Matsuo, *Sci. Technol. Adv. Mater.* 5 (2004) 187.
- [19] T. Omata, S. Otsuka-Yao-Matsuo, *J. Photochem. Photobiol. A: Chem.* 156 (2003) 243.
- [20] Q.H. Zhang, L. Gao, *Acta Chim. Sin.* 63 (2005) 65.
- [21] D.S. Geng, G.X. Lv, Y.S. Bi, Y.P. Bi, *Acta Chim. Sin.* 63 (2005) 658.